The Astronomical Journal, 123:690–701, 2002 February

GLOBULAR CLUSTERS AROUND GALAXIES IN GROUPS

Cristiano Da Rocha and Claudia Mendes de Oliveira
Instituto de Astronomia, Geofísica e Ciências Atmosféricas, Universidade de São Paulo, Avenida Miguel Stefano 4200, 04301-904 São Paulo, SP, Brazil; rocha@iagusp.usp.br, oliveira@iagusp.usp.br

Michael Bolte
Lick Observatory, Department of Astronomy and Astrophysics, University of California, Santa Cruz, California 95064; bolte@ucolick.org

Bodo L. Ziegler
Universitätssternwarte Göttingen, Geismarlandstrasse 11, D-37083 Göttingen, Germany; bziegler@uni-sw.gwdg.de

and

Thomas H. Puzia
Universitätssternwarte München, Scheinerstrasse 1, D-81679 München, Germany; puzia@usm.uni-muenchen.de
Received 2001 August 27; accepted 2001 October 30

ABSTRACT

We have obtained deep photometry of NGC 1199 (in the compact group HCG 22) and NGC 6868 (in the Telescopium loose group) with the Keck II and the ESO VLT-I telescopes. Each galaxy is the optically brightest galaxy of its group. NGC 1199 has two companion galaxies at a median projected distance of only 33 kpc and, based on its peculiar internal structure and large X-ray halo, NGC 6868 has been proposed to be a merger remnant. Our analysis of B and R images uncovered a population of globular clusters around both galaxies, with total (and local) specific frequency $S_N = 3.6 \pm 1.8$ (3.4 ± 1.5) for NGC 1199 and $S_N = 1.8 \pm 1.1$ (0.8 ± 0.4) for NGC 6868. The radial profile of the globular clusters of NGC 1199 follows the light distribution of the galaxy and can be fitted by a power law and a core model with a very steep slope ($\alpha = 2.5 \pm 0.3$). In the case of NGC 6868, the profile of the globular clusters is well fitted by a power law and a core model profile of slope 1.4 ± 0.3 and is shallower than the galaxy light distribution. Maximum likelihood fitting of two Gaussians to the globular cluster color distribution yields a high significance for multimodality, with peaks centered at $(B-R)_0 = 1.13 \pm 0.04$ and 1.42 ± 0.04 (NGC 1199) and $(B-R)_0 = 1.12 \pm 0.07$ and 1.42 ± 0.07 (NGC 6868). NGC 1199 and NGC 6868 are good examples of galaxies in which the group environment is likely to have affected their dynamical evolution. We find that for NGC 1199 the properties of the globular cluster system are similar to those for other systems around external elliptical galaxies located in less dense environments but with a very steep radial profile. In the case of NGC 6868, we find a regular radial profile and color distribution and a comparatively low specific frequency for the globular cluster system of the galaxy.

Key words: galaxies: elliptical and lenticular, cD — galaxies: individual (NGC 1199, NGC 6868) — galaxies: star clusters

1. INTRODUCTION

Variations in the properties of extragalactic globular cluster systems (GCSs) as a function of the environment of the host galaxy hold some of the keys to understanding the formation and evolution of GCSs. Environment has been proposed as one of the important factors in setting the specific frequency S_N (number of clusters normalized by galaxy luminosity). Harris, in a review paper of 1991, pointed out that elliptical galaxies in small groups and sparse environments have on average half the S_N of elliptical galaxies in the Virgo and Fornax clusters (excluding the central galaxies, which have the well-known extremely high specific frequencies). On the other hand Djorgovski & Santiago (1992) found an increase of the S_N with the host galaxy luminosity, which was confirmed by Zepf, Geisler, & Ashman (1994; see Ashman & Zepf 1998; Elmegreen 2000; Harris 2001 for detailed discussion on the subject). As the majority of the very bright galaxies are found in clusters and the faint ones are in groups and in the field, the environmental effect on S_N and its luminosity dependency are not easily disentangled. The effects of host-galaxy environment on other details of the GCSs, the radial and color distributions, are not well documented.

The main goal of this work is to characterize the GCSs of two galaxies in small groups: NGC 1199, the central elliptical galaxy in the compact group HCG 22, and NGC 6868, a suspected merger remnant in the center of the Telescopium group. In particular, we are looking for suggestions that the basic properties of the globular cluster systems around these galaxies have been modified by the dense environment of the compact group or the merger event, respectively.

The compact group HCG 22 contains three bright galaxies. This group was originally cataloged as a quintet of galaxies (Hickson 1982). However, Hickson et al. (1992) showed this to be a triplet at a mean redshift of 0.009 with a superposed discordant pair at $z = 0.0296$. The group has a median velocity of 2686 km s^{-1} and a velocity dispersion of $\sim$54 km s^{-1}. Based on the surface brightness fluctuation method, Tonry et al. (2001) derive a distance modulus $(m-M)_V = 32.6 \pm 0.3$ to NGC 1199, the dominant galaxy of the group, corresponding to 33.1 Mpc, and a median projected galaxy separation in the group of 33 kpc (Tonry et al. 2001 assume $H_0 = 74$ km s^{-1} Mpc^{-1}). NGC 1199 (also known as HCG 22A) is classified as an E2 (Hickson 1982).

NGC 6868 is also classified as an E2 (de Vaucouleurs et al. 1991). The Telescopium group contains five bright galaxies with a median velocity of 2601 km s^{-1} and a velocity

dispersion of ~219 km s^{-1}. Tonry et al. (2001) measure $(m-M)_V = 32.1 \pm 0.2$ based on the surface brightness fluctuation method, which corresponds to a distance of 26.8 Mpc, and a median projected separation for group galaxies of 209 kpc. Although NGC 6868 is located in an environment that has a number density of bright galaxies lower than that of a typical compact group, the interest in studying the globular cluster system of this galaxy is that it is almost certainly a recent merger (Hansen, Jørgensen, & Nørgaard-Nielsen 1991). NGC 6868 appears from its global properties to be an ordinary elliptical galaxy, but in a detailed study Hansen et al. (1991) showed that there are a system of dust features close to the NGC 6868 core and a disk of ionized gas within 1 kpc of its center, indicating the presence of a young population of stars. The kinematics of the gas disk was studied by Plana et al. (1998), who found a flat rotation curve with velocity amplitude ±150 km s^{-1}. The presence of the dust structure and the ionized gas suggest that NGC 6868 may have captured one or more gas-rich galaxies. In addition, NGC 6868 has a halo of X-ray gas associated with it. Its X-ray and optical luminosities are in good agreement with the $L_B - L_X$ relation proposed by Beuing et al. (1999) for early-type galaxies. The general properties of the two galaxies can be seen in Table 1.

The paper is organized as follows. Section 2 describes the observations and data reduction. In § 3 we show the results and § 4 has our discussion.

TABLE 1
GENERAL PROPERTIES OF THE OBSERVED GALAXIES

Parameter	NGC 1199	NGC 6868
l	199.2	350.9
b	−57.3	−32.6
R.A.	$03^h03^m38^s6$	$20^h09^m54^s1$
Decl.	$-15°36'51''$	$-48°22'47''$
Morphological type	E2	E2
B_T	12.5 ± 0.13[a]	11.4 ± 0.11[b]
M_V	-21.3 ± 0.34	-21.9 ± 0.29
$B-V$	0.99[b]	1.00[b]
V_{Rad} (km s^{-1})	2705[b]	2876[b]
Distance[c] (Mpc)	33.1	26.8
Effective Radius	33.″6[d]	38.″4[e]
Int. Vel. Disp.[f] (km s^{-1})	201	277

[a] Hickson et al. 1989.
[b] Faber et al. 1989.
[c] Tonry et al. 2001.
[d] Zepf & Whitmore 1993.
[e] Kobayashi & Arimoto 1999.
[f] Prugniel & Simien 1996.

2. OBSERVATIONS AND DATA REDUCTION

2.1. *Observations*

The images of HCG 22 were obtained with the Keck II telescope in 1997 June using the Low Resolution Imaging Spectrometer (LRIS; Oke et al. 1995). Images in B and R of total exposure times of 720 s (4 × 180) and 630 s (7 × 90) were obtained with an average seeing on the combined images of 0.″77 and 0.″74, respectively. The field size is 5.′7 × 7.′3 and the pixel size is 0.″215. The NGC 6868 images were obtained with the ESO VLT-I in 1999 October using the Focal Reducer/Low Dispersion Spectrograph 1 (FORS1). Images in B and R with total exposure times of 900 s (5 × 180) and 810 s (9 × 90) were obtained with average seeing values on the combined images of 0.″76 and 0.″73, respectively. The field size is 6.′4 × 6.′4 and the pixel size is 0.″2. Images in B and R of similar depth to the ones taken for NGC 6868 were obtained centered on a position 10′ from the galaxy center. This was meant to be our control field for background subtraction. The log of observations is shown in Table 2.

2.2. *Data Reduction*

2.2.1. *Image Processing and Photometry*

Using the IRAF[1] package (Image Reduction and Analysis Facility) we carried out the basic image reduction procedures (bias correction, flat-fielding and image combining). We next used the ELLIPSE and BMODEL of the STSDAS package to model and subtract the light from bright galaxies. We masked the very bright objects on the images and the central regions of the giant galaxies that could not be modeled by ELLIPSE. Subtraction of the sky level of the image was done using the SExtractor package (Source Extractor), Version 2.1.6 (Bertin & Arnouts 1996) with a background mesh size of 64 pixels. The combined images for NGC 1199 and NGC 6868 and the final masked and background-subtracted images are shown in Figure 1.

The combined, masked and background-subtracted images were then used for detection and photometry of the faint objects by using SExtractor with a Gaussian convolution mask of 3 pixels for the HCG 22 images and of 4 pixels for the NGC 6868 images. For photometry of the objects we

[1] IRAF is distributed by the National Optical Astronomy Observatories, which is operated by the Association of Universities for Research in Astronomy, Inc., under cooperative agreement with the National Science Foundation.

TABLE 2
OBSERVATIONAL INFORMATION

Group	Band	Telesc.	Instr.	Date	Tot. Exp. (s)	Pixel Size	No. of Images	Seeing (arcsec)
HCG 22	B	Keck II	LRIS	1997 June 2	720	0.215	4	0.77
HCG 22	R	Keck II	LRIS	1997 June 2	630	0.215	7	0.74
NGC 6868 (1)	B	VLT	FORS1	1999 October 10	900	0.2	5	0.76
NGC 6868 (1)	R	VLT	FORS1	1999 October 10	810	0.2	9	0.73
NGC 6868 (2)	B	VLT	FORS1	1999 October 11	900	0.2	5	0.96
NGC 6868 (2)	R	VLT	FORS1	1999 October 11	810	0.2	9	0.89

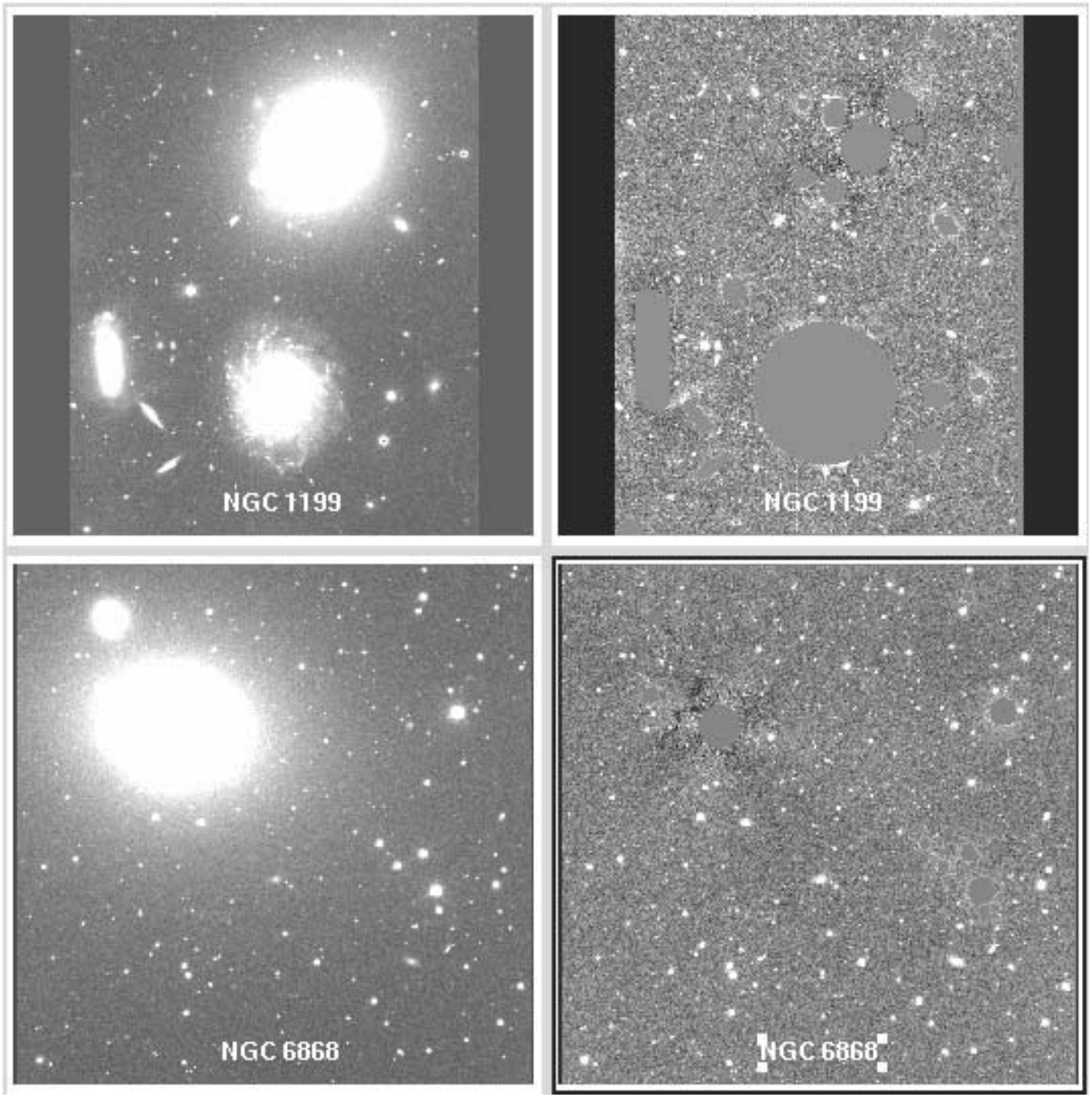

FIG. 1.—*Left*, combined images for HCG 22 (*top*) and NGC 6868 (*bottom*) in the *R* band; *right*, final background-subtracted masked images for HCG 22 (*top*) and NGC 6868 (*bottom*), where the detection and photometry were performed. The field sizes for the top panels are $5\farcm7 \times 7\farcm3$, and for the bottom panels, $6\farcm4 \times 6\farcm4$.

used the MAG_AUTO value, which is given by an adaptive aperture photometry routine, and gives the total magnitude of the detected objects. The adaptive aperture photometry routine is based on the Kron "first moment" algorithm (1980; for more details on the photometry, see Bertin & Arnouts 1996). Monte Carlo simulations were made to test the reliability of the MAG_AUTO photometry (see following section), and a small correction was added to the photometry of each detected object.

The final list of objects includes only the objects that were detected in both *B* and *R* bands. We discarded all the objects that were within $5''$ of the borders of the images and within $5''$ of masked regions.

At the distance of our groups, globular clusters are pointlike sources. To select them, we have excluded the extended objects (dwarf and background galaxies) from our final list. Using the results from the add-star experiments (described in the next section) we could define the range of FWHM in which we expect the pointlike sources to be found, as a function of their magnitudes. The FWHM value is measured by SExtractor. Taking the average FWHM of the simulated objects on the *R* band in 0.5 mag bins and using a 1 σ rejection level, we could determine a "pointlike source locus" on the magnitude-FWHM plane for each image. The detected objects located inside this region, along the magnitude range for each image, were classified as pointlike sour-

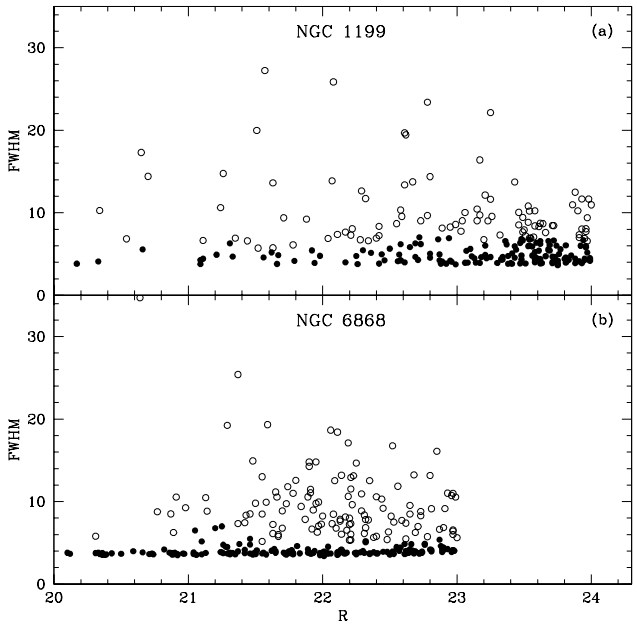

FIG. 2.—Magnitude-FWHM plane used to select pointlike sources, showing the objects classified as pointlike sources (*filled circles*), those classified as extended objects (*open circles*), and objects detected in (*a*) the NGC 1199 images and (*b*) the NGC 6868 images.

ces, and all the other objects were excluded from the final list. This method has shown, in our case, better results than the default SExtractor star-galaxy separations. The selection of pointlike sources using the magnitude-FWHM plane was previously used to select globular cluster (GC) candidates by Rhode & Zepf (2001). The magnitude-FWHM plots for our fields are shown in Figure 2.

Calibration of the images of HCG 22 was done using images from the Cerro Tololo Inter-American Observatory 1.5 m telescope. We have calibrated those HCG 22 images in B and R bands by using Landolt (1992) standard stars and then calibrated the Keck II images by using the surface brightness profile of NGC 1199. The final rms of these calibrations are 0.011 for the B band and 0.016 for the R band. We have checked the calibration by using the surface brightness profiles of NGC 1199 shown in Mendes de Oliveira (1992), and no zero-point differences were found. For NGC 6868 a similar procedure was applied using images from the Las Campanas Observatory 2.5 m telescope and calibrating with Landolt (1992) standard stars. The rms's of these calibrations are 0.003 for the B band and 0.004 for the R band. To obtain the standard-star photometry, we used the packages APPHOT and DAOPHOT.

2.2.2. *Add-Star Experiments*

We used each final image, with bright objects masked out, for an add-star experiment using the IRAF task ADDSTAR in the DAOPHOT package. Our goals were to evaluate the detection completeness, photometric errors, and the limit of the star-galaxy separation method.

We added 600 artificial stellar-like objects to each 0.5 mag bin in the B image, covering the range $18 < B < 28$. In the R image we have added objects in the same position as the ones added to the B image, with $B-R$ colors ranging randomly from 0 to 2.5. The objects were generated from the point-spread function (PSF) for each field. The PSF was constructed using typically 40 to 80 point sources found in the images. These artificial point sources were added in 30 runs of 20 objects each, to avoid artificial crowding of the field. Detection and photometry of the objects in the frames that contained the artificial objects were then performed in the same manner as for the original images. The final simulated object list is composed of the simulated objects recovered in both bands. The number of objects recovered divided by the input number then gave us the completeness fraction. A comparison of the input and output magnitudes of the objects gave us estimates of the random and systematic uncertainties in the photometry.

We have determined the completeness fraction in radial rings centered on the galactic center, and this radial completeness fraction was the one applied in our analyses. This radial dependence is expected since the noise increases in the galaxy-subtracted image as we get close to the center of the galaxy. The radial completeness fractions for both galaxies can be seen in Figure 3. We have also studied the completeness as a function of color and found the variations are at most 5%.

As can be seen in Figure 3, the SExtractor magnitudes are systematically too faint by $\sim$0.05 mag. This difference is expected and is because the aperture correction applied by SExtractor is slightly underestimated for point sources (Bertin & Arnouts 1996). We applied a correction for this light loss to the photometry of detected objects in each frame. The completeness limit for our data given by the add-star experiment was considered to be the magnitude at which at least 80% of the objects were recovered and is shown in Table 3.

3. ANALYSIS AND RESULTS

3.1. *Globular Cluster Luminosity Function*

To select the globular cluster candidates, we have restricted our samples to objects with $22.0 < B < 25.5$ and $20.0 < R < 24.0$ for NGC 1199 and $22.0 < B < 24.5$ and $20.0 < R < 23.0$ for NGC 6868, which represent the ranges of magnitudes in which we expect to observe GCs (the faint limit is given by the completeness limit). We have also applied the color limits $0.7 < (B-R)_0 < 2.1$, the range in which we expect to find the GCs (Thompson & Gregory 1993; Puzia et al. 1999; Woodworth & Harris 2000), eliminating very blue and red unresolved objects.

TABLE 3
DETECTION COMPLETENESS LIMIT WITH THE PERCENTAGE OF CLASSIFICATION

		Detection Completeness	
Image (1)	Band (2)	Mag. Limit (3)	(%) (4)
HCG 22	*B*	25.5	87.5
HCG 22	*R*	24.0	80.0
NGC 6868 (1)...	*B*	24.5	90.2
NGC 6868 (1)...	*R*	23.0	88.9
NGC 6868 (2)...	*B*	24.5	88.3
NGC 6868 (2)...	*R*	23.0	85.7

NOTE.—Col. (1): image name; col. (2): image band; col. (3): completeness limit magnitude; col. (4): percentage of detection at the completeness limit magnitude.

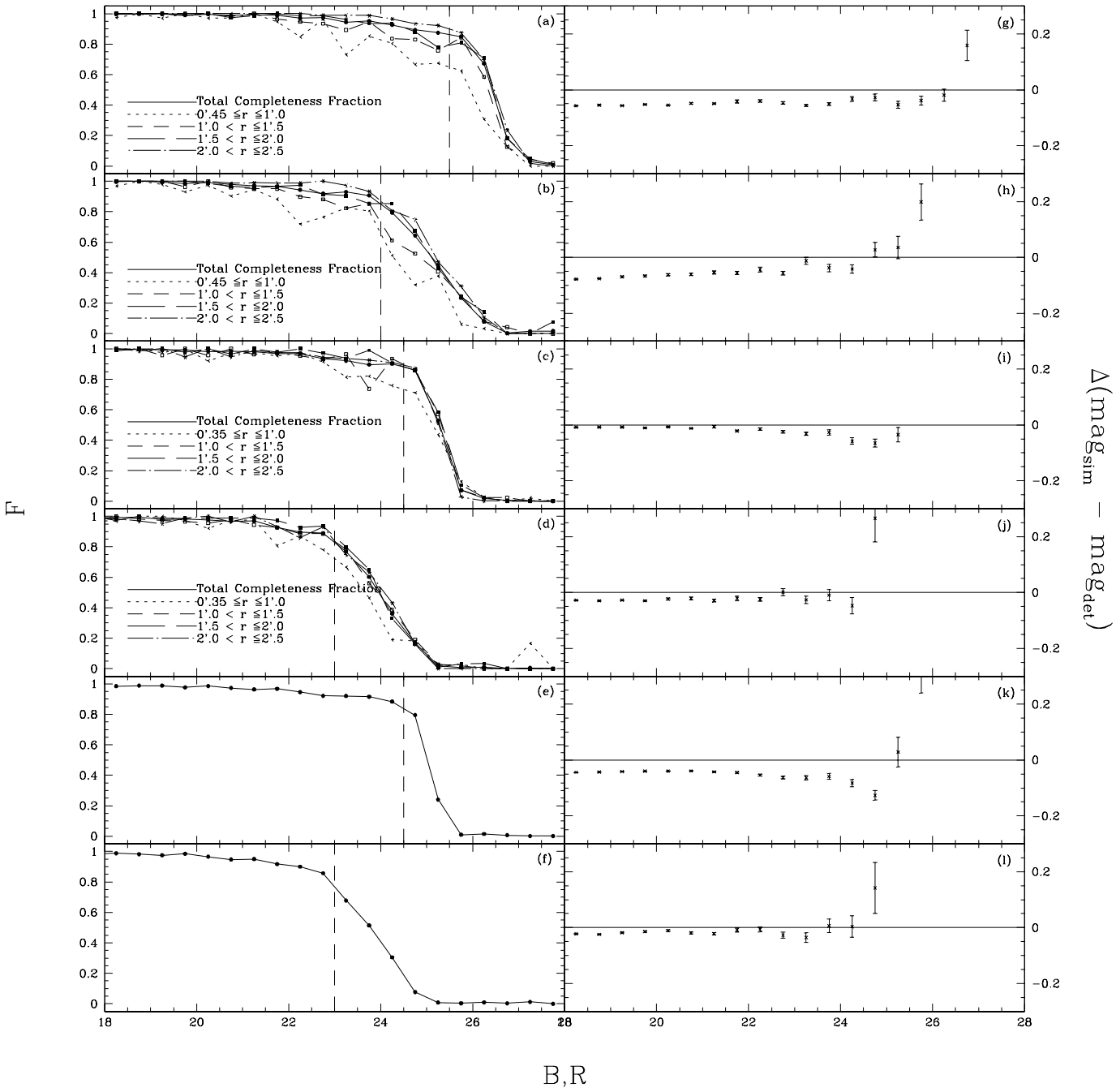

FIG. 3.—*Left*: Detection completeness fractions estimated with the add-star experiment performed in the six images of our study, showing the faint magnitude limit considered in each sample (*vertical dashed lines*). Total and radial completeness fractions for the HCG 22 images in (*a*) the *B* band and (*b*) the *R* band; fractions for the NGC 6868 images in (*c*) the *B* band and (*d*) the *R* band; total completeness fraction for the NGC 6868 background fields in (*e*) the *B* band and (*f*) the *R* band. *Right*: Photometric errors estimated with the add-star experiment. Errors for the HCG 22 images in (*g*) the *B* band and (*h*) the *R* band; errors for the NGC 6868 images in (*i*) the *B* band and (*j*) the *R* band; errors for the NGC 6868 background fields in (*k*) the *B* band and (*l*) the *R* band.

For our selected sample, we plot the number density as a function of distance from the center of the galaxies (see Fig. 4). In those plots we can clearly see at which radius the background level for the objects was reached. Counting objects in rings of 0.″2 and correcting the counts for incompleteness, we can see that the radial profile reaches the background counts at distances larger than 2.″4 from the center of NGC 1199. For NGC 6868 we have counted objects in rings of 0.″5. The counts in the background field (for radii greater than 10′ in Fig. 4) are approximately constant, and these are taken to represent the background counts for this group. The error bars represent the Poissonian error on the number counts.

We have used the flat region between 2.″4 (23 kpc) and 4.″2 (40 kpc) around NGC 1199 to estimate the background level. We do not have control fields taken away from the group center to make a background estimation in another way. From Figure 4 we note that there is a central concentration of objects within a radius of 2.″4 from the center of NGC 1199. We identify this concentration with the GCS of

this galaxy. A similar analysis was applied to NGC 1190 (HCG 22B) and NGC 1189 (HCG 22C), and no significant central concentration of pointlike sources was found around them. From their morphological types (Sa and SBcd) and their luminosities ($M_V = -18.7$ and $M_V = -19.6$; Hickson, Kindl, & Auman 1989) they are not expected to have a large GC population (Harris 1991; Ashman & Zepf 1998).

We can also see a high concentration of objects around the center of NGC 6868, as is shown in Figure 4. At galactocentric distances larger than 10′ (or 78 kpc; objects located on the second field), we have a flat region, which is used as the background control field. We regard as our sample of possible candidate globular clusters of NGC 6868 the objects within a distance of 3.′8 (30 kpc) of the center of the galaxy (within the magnitudes and color limits previously defined). The objects within an annulus of inner radius 10′ and outer radius 17′ were considered to belong to a sample of background galaxies and foreground stars (within the same limits).

We will, hereafter, refer to the area within 2.′4 from the center of NGC 1199 and 3.′8 from the center of NGC 6868 as the "on-galaxy region" or "studied area," and to the region within 2.′4 and 4.′2 from the center of NGC 1199 and the field taken 10′ from the center of NGC 6868 as the "background area."

Since we do not have an independent background field for NGC 1199, we have estimated the number of foreground stars in the direction of the galaxy by using the galactic model by Santiago, Gilmore, & Elson (1996). We found that in the magnitude range of the globular clusters, the possible contamination of our sample by foreground stars is 0.4 objects arcmin^{-2}, which gives us only 5.5 objects in the studied area. This estimate of foreground stars is negligible, and the number of GCs found around NGC 1199 could not be much affected by a wrong stellar contamination estimate in our small area background field. However, by far, background galaxies are the largest source of contamination. The background field used for NGC 1199 (the outskirts of the field) gives a statistically more uncertain background subtraction and can still contain bona fide GCs that will be counted as background objects (although Fig. 4 shows a very flat profile beyond a distance of 2.′4 from the center of the galaxy). In the case of NGC 6868, since the estimate of the number of foreground and background objects was done using an independent frame of the same size as that of the on-galaxy frame, obtained at a distance of 10′ to the center of the galaxy, the background subtraction is more reliable.

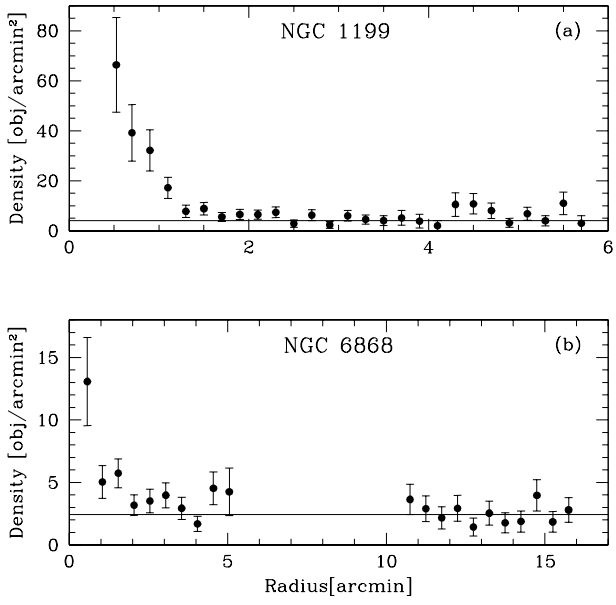

FIG. 4.—Radial profile of objects classified as pointlike sources within the magnitudes and color limits $[0.7 \leq (B-R)_0 \leq 2.1]$. (*a*) Distribution of objects around NGC 1199, from 0′ to 6′ in rings of 0.′2. The magnitude ranges are $B = 22.0$ to 25.5 and $R = 20.0$ to 24.0. (*b*) Distribution of objects around NGC 6868, from 0′ to 17′ in rings of 0.′5. The magnitude ranges are $B = 22.0$ to 24.5 and $R = 20.0$ to 23.0. The solid lines represent the estimated background level: 4.2 objects arcmin^{-2} for NGC 1199 and 2.4 objects arcmin^{-2} for NGC 6868. Note the different scales for the top and bottom distributions.

The globular cluster luminosity function (GCLF) was built by binning the GC candidates by 0.5 mag. The number counts were corrected for incompleteness by dividing the number counts in each bin by the completeness fraction. The photometric errors were neglected, and the errors for the corrected number counts were given by

$$\sigma^2 \approx \left[\frac{N_{\rm obs}}{f^2} + \frac{(1-f)N_{\rm obs}^2}{N_{\rm add}\, f^3} \right], \qquad (1)$$

where $N_{\rm obs}$ is the number of objects detected in the image, $N_{\rm add}$ is the number of objects added to the image in the add-star experiment, and f is the completeness fraction to this magnitude bin (Bolte 1994).

The corrected number counts for the on-galaxy region were reduced by the corrected background number counts normalized to the sampled area. For NGC 1199, we have selected 128 ± 11 objects, which, corrected for incompleteness, gives 158 ± 14 objects, in an area 13.7 arcmin^2. In the background, for the same area, we have a corrected number count of 61 ± 10 objects, leaving a net number count of 97 ± 18 objects. For NGC 6868, there are 111 ± 10 selected objects, which corresponds to 124 ± 12 objects when corrected for incompleteness, in an area of 27.2 arcmin^2. In the background we have a corrected number count of 74 ± 8 objects in the same area, resulting in a net number count of 50 ± 14 objects.

The luminosity function of globular clusters around giant elliptical galaxies has been well studied in the literature. It is generally accepted that it can be well approximated by a Gaussian distribution function. For the peak (turnover magnitude$-m_0$) and the dispersion we have used the typical values for elliptical galaxies, $M_V = -7.33 \pm 0.04$ and $\sigma = 1.40 \pm 0.05$ (Harris 2001).

The galactic extinction is the same for both galaxies, $E(B-V) = 0.056$ (Schlegel, Finkbeiner, & Davis 1998). With the reddening laws found in Rieke & Lebofsky (1985) we have $A_B = 0.23$, $A_R = 0.13$, and $E(B-R) = 0.10$.

Using the distance moduli for our galaxies and the reddening corrections above, we expect to start seeing the brightest GCs for NGC 1199 at $B = 22.5$ and $R = 20.9$, and the turnover at $B = 26.2 \pm 0.3$ and $R = 24.6 \pm 0.3$. For NGC 6868, $B = 22.1$ and $R = 20.5$ for the brightest GCs, and $B = 25.7 \pm 0.2$ and $R = 24.1 \pm 0.2$ for the turnover magnitude. As we do not reach the turnover point of the GCLF with our data, we did not attempt to fit the peak and the dispersion values, leaving only the normalization of the

TABLE 4
GAUSSIAN-FIT PARAMETERS

Image (1)	Band (2)	m_0 (3)	χ^2 (4)	% (5)
HCG 22	*B*	26.2 ± 0.3	0.3214	30.8 ± 8.5
HCG 22	*R*	24.6 ± 0.3	0.2630	33.4 ± 8.7
NGC 6868...	*B*	25.7 ± 0.2	0.2854	18.7 ± 5.3
NGC 6868...	*R*	24.1 ± 0.2	0.1995	20.9 ± 5.2

NOTE.—Col. (1): image name; col. (2): image band; col. (3): peak position (fixed at $M_V = -7.33$); col. (4): χ^2 of the Gaussian fit; col. (5): area of Gaussian covered by our data.

Gaussian as a free parameter. The χ^2 of the fits and the area of the Gaussians covered by our data for both galaxies are seen in Table 4 and Figure 5.

3.2. *Specific Frequency and Radial Profile Modeling*

The specific frequency (S_N), as defined by Harris & van den Bergh (1981), is the number of objects normalized by the galaxy luminosity:

$$S_N \equiv N_{GC} 10^{0.4(M_V+15)}. \quad (2)$$

Using a Gaussian fit for the GCLF we can determine the part of the GC population that we are measuring and extrapolate the number of GCs over all magnitudes in our image. With the number of GCs found in the on-galaxy areas (local number) and the light in the same area where the GCs were counted, we can calculate the "local specific frequency" (S_{N_l}), i.e., the specific frequency of the GCs that are detected in our images.

Correcting the number counts of NGC 1199 for the unobserved part of the GCLF we have a total number of 314 ± 105 GCs over all magnitudes. The galaxy light, estimated using the ELLIPSE model in the same area, is $V = 12.9 \pm 0.2$ or $M_V = -19.9 \pm 0.3$. Using those values to calculate the local specific frequency (S_{N_l}) for NGC 1199 we have 3.4 ± 1.5. Applying the same procedure for NGC 6868 the local number of GCs over all magnitudes is 266 ± 106 and the light in this area is $V = 11.0 \pm 0.2$ or $M_V = -21.3 \pm 0.3$, which gives $S_{N_l} = 0.8 \pm 0.4$. The errors on S_N include the error on the number counts, background subtraction, GCLF extrapolation and uncertainties in its parameters, the photometric error on the galaxy magnitude, and the error in the distance of the galaxy.

We now determine the global specific frequency (S_{N_g}) for the system. S_{N_g} is calculated using the extrapolation of the radial profile to estimate a total number of GCs for each galaxy and the total light of the galaxy.

To estimate the total number of objects in the GCS, the sample was divided in radial rings of 0.′2 for NGC 1199 and 0.′5 for NGC 6868. The number of GC candidates in each radial ring was corrected for the lost area due to the masks and unobserved regions. We then calculated the total num-

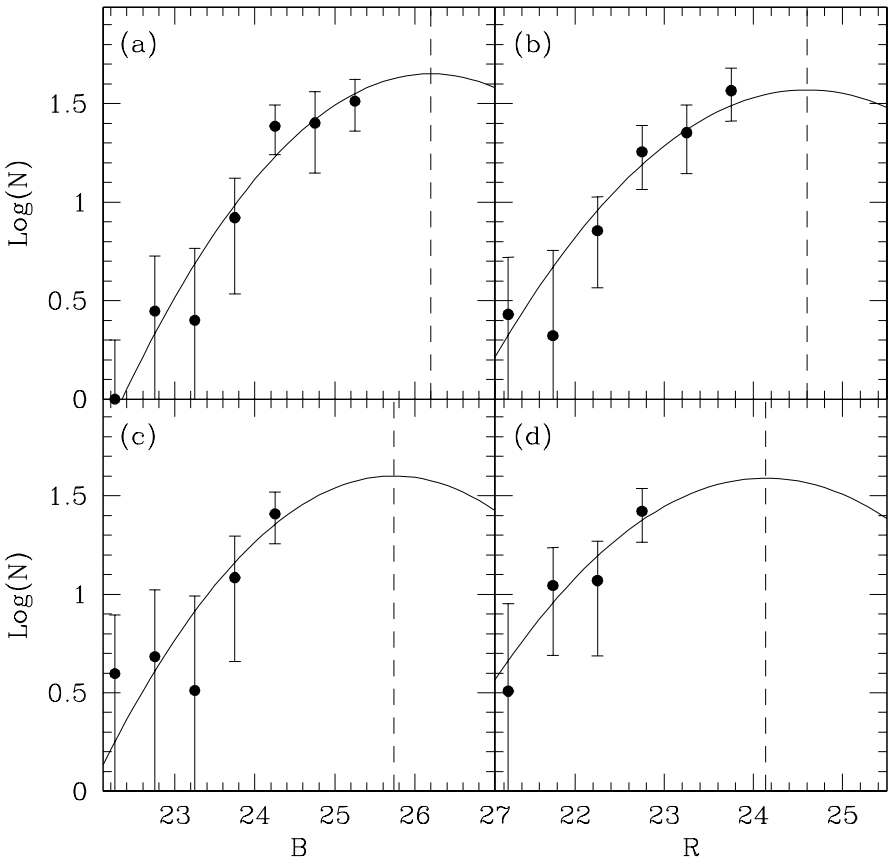

FIG. 5.—Globular cluster luminosity functions. Luminosity function of the globular cluster system around NGC 1199 in (*a*) the *B* band and (*b*) the *R* band. Luminosity function of the globular cluster system around NGC 6868 in (*c*) the *B* band and (*d*) the *R* band. The solid line represents the Gaussian fit, and the dashed lines, the expected turnover magnitudes.

ber of GCs over all magnitudes in the complete ring from the central mask and the limiting galactocentric distance. We use two different radial profiles. The first one is a variation of the core model profile proposed by Forbes et al. [1996; $\rho = \rho_0(r_c^\alpha + r^\alpha)^{-1}$] with the core radius estimated for the GCSs of elliptical galaxies by the relation shown in the same work [$r_c = -(0.62 \pm 0.1)M_V - 11.0$, where r_c is in kiloparsecs]. This core model profile is a simplified analytic form of the King profile (King 1962). The other profile is a power-law profile ($\rho \propto r^{-\alpha}$).

For either profile the best-fitting model was determined and the total number of GCs estimated by integrating the profiles. For NGC 1199 the profile was constrained by the corrected number counts between 0′.45 and 2′.4. For NGC 6868 the fitted range was 0′.35 to 3′.8. Table 5 and Figure 6 summarize the fits.

For NGC 1199 the slope of the power-law profile is 2.5 ± 0.3, which is very steep, and therefore the total number of GCs is dominated by the central region. To be able to integrate this profile, we have set a minimum inner radius of 0′.1 (∼1 kpc). We assume that there is no contribution inside this radius since the GCs in this region were probably destroyed by erosion processes. This mathematical artifact gives an upper limit for the total population of GCs. For NGC 6868 the slope of the best-fit power-law profile is 1.4 ± 0.3, and it can be integrated analytically (see results below). The slopes used in the core model profile are the same as used in the power-law profile.

TABLE 5
SPECIFIC FREQUENCY VALUES

Galaxy (1)	N (2)	S_n (3)
NGC 1199:		
Local.....	314 ± 105	3.4 ± 1.5
$r_c = 2.19$.....	1169 ± 429	3.6 ± 1.8
$\alpha = 2.5 \pm 0.3$	1668 ± 899	5.2 ± 3.2
NGC 6868:		
Local.....	266 ± 106	0.8 ± 0.4
$r_c = 2.58$.....	1060 ± 555	1.8 ± 1.1
$\alpha = 1.4 \pm 0.3$	1089 ± 503	1.9 ± 1.0

NOTE.— Col. (1): estimated local values, core radius value in kiloparsecs for the core model profile and slope of the power-law profile; col. (2): estimated number of globular clusters; col. (3): estimated specific frequency.

The total number of GCs for each galaxy estimated by the two kinds of profiles can be seen in Table 5, and the radial profiles of GC candidates with the power-law and core model profiles used and the galaxy light overplotted are shown in Figure 6. The assumption about the profile shape is very important because we have to extrapolate the number counts in the outer and inner parts of the galaxy.

The profiles were extrapolated to 100 kpc, which is the maximum radius to which we expect the GCS to extend.

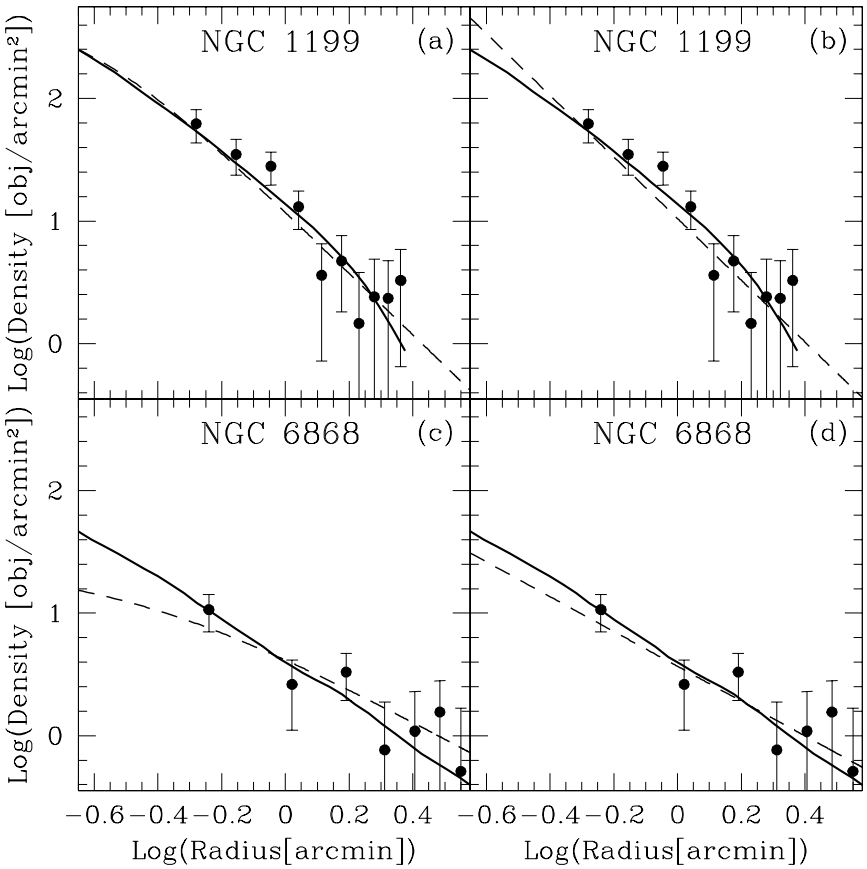

FIG. 6.—Radial profiles of globular cluster candidates. (*a*) Radial profile of the candidates around NGC 1199 with the fitted core model profile with the best-suited core radius (Forbes et al. 1996; *dashed line*) and overplotted with the galaxy light in the *B* band, arbitrarily vertically shifted (*continuous line*); (*b*) radial profile of the GCS around NGC 1199 and the galaxy light (*continuous line*) with the power-law profile (*dashed line*) overplotted; (*c*) and (*d*) same as (*a*) and (*b*), respectively, but for the candidates around NGC 6868.

Rhode & Zepf (2001) do not detect GCs farther than 100 kpc in NGC 4472, which is at least twice as luminous as the galaxies in our sample. Three sources of error were considered on the radial profile extrapolation using the core model: the errors on the slope, on the core radius, and on the outer radius cutoff. To estimate the error we make by cutting the profiles at the outer radius (100 kpc) we have calculated the change in the results caused by varying the outer radius cutoff by 20%. For NGC 1199, in which the numbers are dominated by the inner region, the error on S_N is 0.06, and for NGC 6868 is 0.2. The error introduced in the S_N by a 30% variation of the core radius is 0.6 for NGC 1199 and only 0.04 for NGC 6868, for which the numbers are dominated by the outer region.

For the extrapolation using the power-law profile three sources of error were also considered: the error in the slope and the outer radius cutoff, in the same manner as for the "core radius" extrapolation, and the error in the inner radius cutoff, for the case of NGC 1199. We have varied the inner radius cutoff (1 kpc) by 50% to estimate the error we make in the cut, which translated into an error for S_N of 1.8. The errors caused by all the sources, for both models, were added in quadrature and are shown in Table 5.

To calculate S_{N_g} we have used the total magnitude of the galaxies and the total number of GCs obtained through the integration of the two kinds of profiles. The results are shown in Table 5 and are discussed in § 4.

3.3. *GC Color Distribution*

Bimodal color distributions of GCs are found in at least 50% of elliptical galaxies (Gebhardt & Kissler-Patig 1999; Kundu & Whitmore 2001) and even in some spiral galaxies such as our own and M31 (Ashman & Zepf 1998; Harris 2001, and references therein). They are thought to be due to multiple events of star formation in the galaxies' histories. This effect was predicted for elliptical galaxies by the Ashman & Zepf (1992) merger model and was first detected in NGC 4472 and NGC 5128 (Zepf & Ashman 1993). Since then other models such as the multiple-collapse model (Forbes, Brodie, & Grillmair 1997) and the accretion model (Côté, Marzke, & West 1998; Hilker, Infante, & Richtler 1999) appeared to explain it. Since we are searching for modifications in the GCS properties caused by the small-group environment, multimodal color distributions of GCs may give some useful information about the GCS history.

The color distribution of all the objects detected in the on-galaxy areas is analyzed here, with no attempt to perform a background subtraction. The color distributions of the background objects, which can be seen in Figure 7, are very broad, with one dominant peak. The peak positions are not located at the same place as the GC candidates peaks (see Fig. 8). Therefore, we do not expect the shape of the background color distribution to affect our analysis.

We have applied a KMM test (Ashman, Bird, & Zepf 1994) to detect and estimate the parameters of possible bimodalities in the color distributions. The KMM code uses maximum likelihood to estimate the parameters that best describe the sample distributions for a single-Gaussian fit and for multiple-Gaussian fits and calculates the probability of the single Gaussian being the best fit for the sample distribution. This code can be run in two modes, homoscedastic, which finds groups with the same covariance values, and heteroscedastic, which finds groups with dissimilar covariance values. The last mode has reliability problems with the analytic approximation to the significance level, and for this reason it is not commonly used for this kind of analysis.

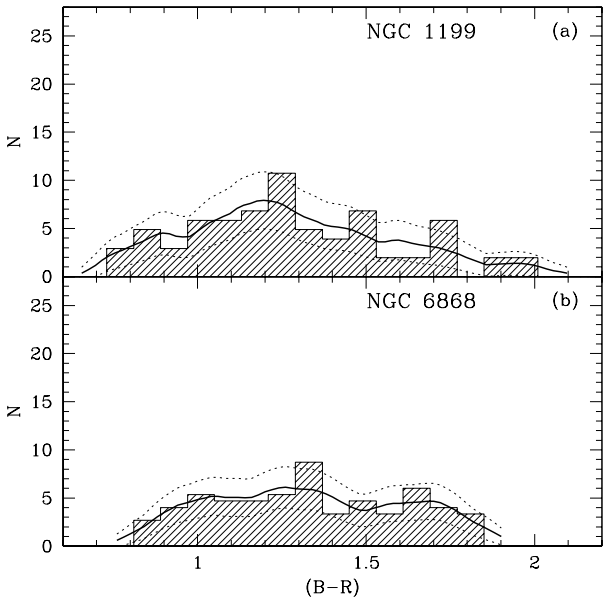

FIG. 7.—Color distribution of background objects for (*a*) NGC 1199 and (*b*) NGC 6868, showing the distribution function derived by the Epanechnikov kernel density estimator (*solid line*) and its upper and lower limits (*dotted lines*).

Running KMM in the homoscedastic mode on our color distributions yields the two-Gaussian option as the result with 99.9% confidence level for both galaxies. For NGC 1199 the peaks are located at $(B-R)_0 = 1.13 \pm 0.04$ and $(B-R)_0 = 1.42 \pm 0.04$ with 62% of the GCs on the blue peak and 38% on the red one and a covariance of 0.01. For

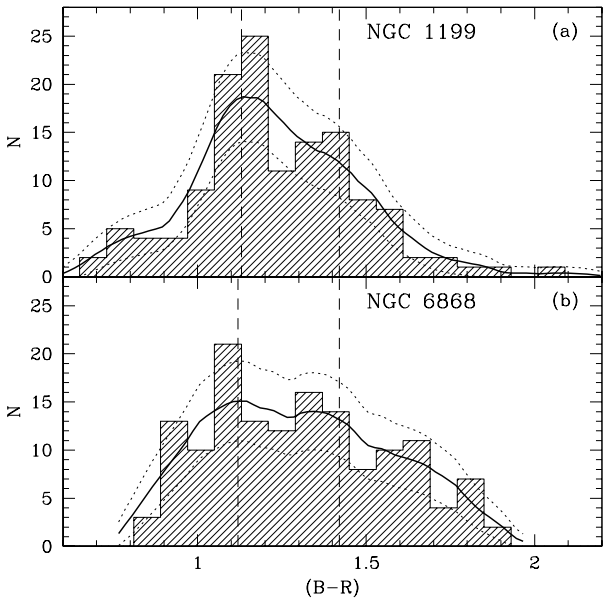

FIG. 8.—Color distribution of globular cluster candidates (no background subtraction is done), showing the color distribution of objects around (*a*) NGC 1199 and (*b*) NGC 6868, the distribution function derived by the Epanechnikov kernel density estimator (*solid line*), its upper and lower limits (*dotted lines*), and the peak values found by KMM (*vertical dashed lines*).

NGC 6868 the values found are $(B-R)_0 = 1.12 \pm 0.07$ and $(B-R)_0 = 1.42 \pm 0.07$ with 51% of the GCs on the blue peak and 49% on the red peak and a covariance of 0.009. The errors represent the mean error on the peak position given by the KMM added in quadrature with the mean photometric errors of the colors.

A visual inspection of the color histograms and the estimates using the Epanechnikov kernel density estimator (see Silverman 1986 for detailed discussion on the kernel density estimator) shows that there might be a bimodality for NGC 1199 and that there are, at least, two major peaks for NGC 6868. The KMM results, bimodality significance, and the peak positions are in good agreement with the visual inspections and the kernel density estimates, as can be seen in the distributions in Figure 8.

Splitting the GC candidates into blue and red subsamples, we have analyzed the radial distribution of each subpopulation and found that the red clusters are more centrally concentrated than the blue ones, as found in the literature (Geisler, Lee, & Kim 1996; Kissler-Patig et al. 1997; Lee, Kim, & Geisler 1998; Kundu & Whitmore 1998). The slopes found by fitting a power law to the radial profiles are 2.2 ± 0.4 and 2.9 ± 0.6 to the blue and red subpopulations of NGC 1199, respectively, and 0.8 ± 0.4 and 1.7 ± 0.2 to the blue and red subpopulations of NGC 6868, respectively.

4. DISCUSSION AND CONCLUSIONS

We present a short summary of the results we have found so far before we proceed with the discussion:

1. We detect a significant population of centrally concentrated GCs around the galaxies NGC 1199 and NGC 6868, as shown in Figure 4.
2. The two first-ranked group galaxies studied here show different S_N values. For NGC 1199, S_N appears to be "normal" for an elliptical galaxy, while for the suspected merger NGC 6868, the specific frequency is somewhat low compared with other galaxies of similar luminosities.
3. We find a good case for bimodal color distributions in the populations of GCs, and in both cases the radial distributions for the red objects have steeper slopes than those for the blue objects.

In the following we will further discuss these main results and will attempt to fit our observations into what is known about GC systems around other elliptical galaxies.

4.1. *Radial Profiles and Population Sizes*

The radial profiles shown in Figure 4 show a central concentration of objects within 2.′4 (23 kpc) of the center of NGC 1199 and 3.′8 (30 kpc) of the center of NGC 6868, indicating the existence of a significant population of globular clusters around these galaxies.

NGC 1199 has a very steep radial profile that follows the galaxy light and can be fitted by a power law with $\alpha = 2.5 \pm 0.3$ and by a core model profile with the same slope and core radius $r_c = 2.19$ kpc. The light profile of NGC 1199 is as steep as the radial distribution of GCs out to a radius of 1.′5 and then it becomes steeper. Using our determination of the global specific frequency for this galaxy done with the core model profile, our value of S_N can be taken only as an upper limit, if the real profile of the GCSs follows that of the light of the galaxy exactly. The steep profile can be caused by the destruction of the outer part of the system by tidal effects, since we have two giant galaxies closer than 35 kpc and with small relative velocities, or by some inefficiency of the erosion processes in the inner part of the galaxy. The estimated global specific frequency (3.6 ± 1.8 using the core model and 5.2 ± 3.2 using the power-law model) is similar to the "normal" value for elliptical galaxies, where the "normal" value is defined as a typical value for elliptical galaxies as given by Harris (2001). There is no optical sign of star formation regions in the galaxy that could artificially change the S_N value.

The GCS of NGC 6868 has a regular radial profile; the slope of the power law fitted to the distribution is $\alpha = 1.4 \pm 0.3$. The value of the slope for a power-law radial profile of GCs for a normal elliptical galaxy ranges from 1 to 2 (Ashman & Zepf 1998). The GCS profile is more extended than the galaxy light, which has a slope of 1.72, as can be seen in Figure 6. Our final result for the global specific frequency for this galaxy is $S_N = 1.8 \pm 1.1$, assuming a core model profile, and 1.9 ± 1.0, assuming the power-law profile. This value is lower, by almost a factor of 2, than the "normal" value of Harris (2001) for an elliptical galaxy ($S_N \sim 3.5$) and indicates a poor GCS (although it's well known that the scatter in the values of S_N for elliptical galaxies is large). This might be due to a high efficiency of forming stars in the past as opposed to the formation of globular clusters or to very efficient destruction mechanisms that could perhaps be related to the recent merger that may have occurred in the central part of the galaxy (Hansen et al. 1991). As for NGC 1199, there are no obvious signs of widespread star formation throughout the galaxy that could affect the S_N value of NGC 6868.

4.2. *Colors of the GC Population*

According to stellar population evolutionary synthesis models (Worthey 1994; Bruzual & Charlot 1993) metallicity effects are supposed to dominate color differences in globular clusters if the populations are older than 1 Gyr. We expect the bulk of the populations of GCs to be older than 1 Gyr, since we could not find evidences of recent star formation. A linear relation between the color and the metallicity is predicted by the population synthesis models as the relation proposed by Reed, Harris, & Harris (1994; $[\mathrm{Fe/H}] = 3.112(B-R)_0 - 4.967$, $\sigma[\mathrm{Fe/H}] = 0.21$).

Some studies have found doubly peaked color distributions of GCSs around elliptical galaxies. Gebhardt & Kissler-Patig (1999) and Kundu & Whitmore (2001), respectively, found for samples of 43 and 29 early-type galaxies observed with the *Hubble Space Telescope* (*HST*) that at least 50% of the elliptical galaxies have GCSs with bimodal color distributions. Studies of the GCS of NGC 4472 (M49; Geiser et al. 1996; Lee et al. 1998; Puzia et al. 1999) have found color distributions with peak metallicities corresponding to $[\mathrm{Fe/H}] = -1.5 \pm 0.05$ dex and $[\mathrm{Fe/H}] = -0.32 \pm 0.05$ dex by using the color-metallicity relation given by Kundu & Whitmore [1998; $[\mathrm{Fe/H}] = -(4.50 \pm 0.30) + (3.27 \pm 0.32)(V-I)$]. Neilsen & Tsvetanov (1999) in a study of 12 Virgo elliptical galaxies found a bimodal color distribution for the GCSs around eight of them.

The recent work of Larsen et al. (2001), presents an analysis of 17 nearby early-type galaxies, homogeneously observed with *HST*. In this work they have found a

correlation between the GCS mean color and the luminosity and the mean color and the velocity dispersion of the host galaxy. Strong correlations were found for the red peaks, which were also found by Forbes et al. (1997) and by Forbes & Forte (2001). The latter study suggested the following color–velocity dispersion relation: $V-I = 0.23 \log \sigma + 0.61$. Weak correlations were found for the blue peaks and were discarded by the previously cited works. Burgarella, Kissler-Patig, & Buat (2001) have found an average metallicity of [Fe/H] $= -1.4$ dex for the blue peak, which agrees with the average value found previously by other authors. Kundu & Whitmore (2001) found that the correlations for both peaks are, at best, weak. In general, the average metallicity of the globular clusters in a bimodal distribution, when considered as a single population, is in agreement with the value of a unimodal distribution ([Fe/H] $= -1.0 \pm 0.05$ dex; Kundu & Whitmore 2001). The GCSs around the two galaxies studied here were analyzed with the KMM code (Ashman et al. 1994), which has detected bimodal populations for the GCSs around NGC 1199 and NGC 6868.

For NGC 1199, KMM has located peaks at $(B-R)_0 = 1.13 \pm 0.04$ and $(B-R)_0 = 1.42 \pm 0.04$, which corresponds to [Fe/H] $= -1.45 \pm 0.21$ dex and [Fe/H] $= -0.55 \pm 0.21$ dex, respectively (Reed et al. 1994), similar to the values found for many published galaxies in the last years, as seen in the following. Transforming our $B-R$ values to $V-I$, using the relation given by Forbes & Forte [2001; $V-I = 0.68(B-R) + 0.15$], and overplotting them (*large filled symbols*) on the Forbes & Forte (2001) color–velocity dispersion plot (Fig. 9), we can see that our results are consistent with theirs and those of other studies.

For NGC 6868, peaks found by KMM are located at $(B-R)_0 = 1.12 \pm 0.07$ and $(B-R)_0 = 1.42 \pm 0.07$, corresponding to [Fe/H] $= -1.48 \pm 0.22$ and [Fe/H] $= -0.55 \pm 0.22$ dex, respectively (Reed et al. 1994). Those values are also in agreement with the ones found for many galaxies in the literature. In Figure 9 we can see our measured values overplotted on the diagram of Forbes & Forte (2001; *large open symbols*).

The results reported in this work show that there is a need of more work on globular cluster systems around small-group elliptical galaxies to understand the effects to which the GCSs are exposed in such an environment.

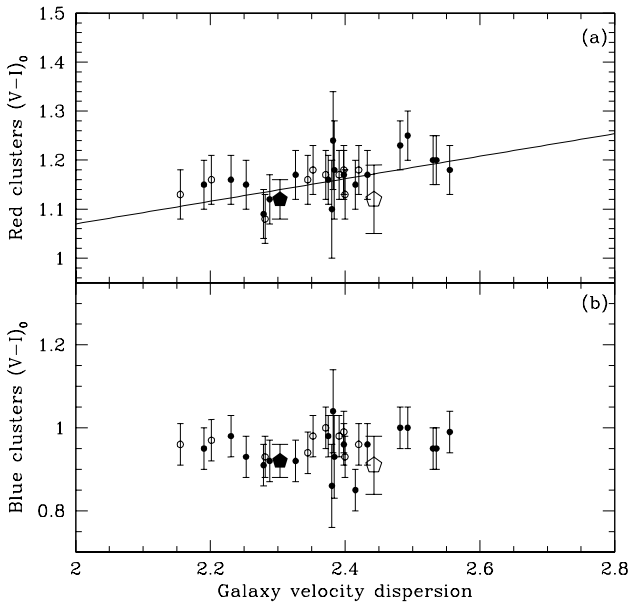

FIG. 9.—Color–velocity dispersion relation for the early-type galaxies of Forbes & Forte (2001), showing values for (*a*) the red peaks and (*b*) the blue peaks, the color–velocity dispersion relation proposed by Forbes & Forte (2001; *solid line*), and the values for NGC 1199 (*filled pentagons*) and NGC 6868 (*open pentagons*).

C. D. R. is supported by FAPESP (Fundação de Amparo a Pesquisa do Estado de São Paulo) Ph.D. grant 96/08986-5. C. M. O. acknowledges support from FAPESP. M. B. is happy to acknowledge support from National Science Foundation grant AST 99-01256. B. L. Z. acknowledges support from the Deutsche Forschungsgemeinschaft and the VW foundation. T. H. P. gratefully acknowledges the financial support during his visit at Universidade de São Paulo. We are grateful to Mike West, Basílio Santiago, Arunav Kundu, and Keith Ashman, the referee, for careful reading of this manuscript and useful comments to improve its content, and to Héctor Cuevas and Leopoldo Infante for observing the standard stars for calibration of the NGC 6868 field.

REFERENCES

Ashman, K. M., Bird, C. M., & Zepf, S. E. 1994, AJ, 108, 2348
Ashman, K. M., & Zepf, S. E. 1992, ApJ, 384, 50
———. 1998, Globular Cluster Systems (Cambridge Univ. Press)
Bertin, E., & Arnouts, S. 1996, A&AS, 117, 393
Beuing, J., Döbereiner, S., Böhringer, H., & Bender, R. 1999, MNRAS, 302, 209
Bolte, M. 1994, ApJ, 431, 223
Bruzual, G. A., & Charlot, S. 1993, ApJ, 405, 538
Burgarella, D., Kissler-Patig, M., & Buat, V. 2001, AJ, 121, 2647
Côté, P., Marzke, R. O., & West, M. J. 1998, ApJ, 501, 554
de Vaucouleurs, G., de Vaucouleurs, A., Corwin, H. G., Buta, R. J., Paturel, G., & Fouqué, P. 1991, Third Reference Catalogue of Bright Galaxies (New York: Springer)
Djorgovski, S., & Santiago, B. X. 1992, ApJ, 391, L85
Elmegreen, B. 2000, in Toward a New Millennium in Galaxy Morphology, ed. D. L. Block, I. Puerari, A. Stockton, & D. Ferreira (Dordrecht: Kluwer), 269–270, 469
Faber, S., Wegner, G., Burnstein, D., Davies, R. L., Dressler, A., Lynden-Bell, D., & Terlevich, R. J. 1989, ApJS, 69, 763
Forbes, D. A., Brodie, J. P., & Grillmair, C. J. 1997, AJ, 113, 1652
Forbes, D. A., & Forte, J. C. 2001, MNRAS, 322, 257
Forbes, D. A., Franx, M., Illingworth, G. D., & Carollo, C. M. 1996, ApJ, 467, 126
Gebhardt, K., & Kissler-Patig, M. 1999, AJ, 118, 1526
Geisler, D., Lee, M. G., & Kim, E. 1996, AJ, 111, 1529
Hansen, L., Jørgensen, H. E., & Nørgaard-Nielsen, H. U. 1991, A&A, 243, 49
Harris, W. E. 1991, ARA&A, 29, 543
———. 2001, in Lectures for the 1998 Saas Fee Advanced School on Star Clusters, ed. L. Labhardt & B. Binggeli (Course 28) (Berlin: Springer), 223
Harris, W. E., & van den Bergh, S. 1981, AJ, 86, 1627
Hickson, P. 1982, ApJ, 255, 382
Hickson, P., Kindl, E., & Auman, J. R. 1989, ApJS, 70, 687
Hickson, P., Mendes de Oliveira, C., Huchra, J. P., & Palumbo, G. G. 1992, ApJ, 399, 353
Hilker, M., Infante, L., & Richtler, T. 1999, A&AS, 138, 55
King, I. R. 1962, AJ, 67, 471
Kissler-Patig, M., Richtler, T., Storm, J., & Della Valle, M. 1997, A&A, 327, 503
Kobayashi, C., & Arimoto, N. 1999, ApJ, 527, 573
Kron, R. G. 1980, ApJS, 43, 305
Kundu, A., & Whitmore, B. C. 1998, AJ, 116, 2841
———. 2001, AJ, 121, 2950
Landolt, A. U. 1992, AJ, 104, 340
Larsen, S. S., Brodie, J. P., Huchra, J. P., Forbes, D. A., & Grillmair, C. 2001, AJ, 121, 2974
Lee, M. G., Kim, E., & Geisler, D. 1998, AJ, 115, 947

Mendes de Oliveira, C. L. 1992, Ph.D. thesis, Univ. British Columbia
Neilsen, E. H., & Tsvetanov, Z. I. 1999, ApJ, 515, L13
Oke, J. B., et al. 1995, PASP, 107, 375
Plana, H., Boulesteix, J., Amram, Ph., Carignan, C., & Mendes de Oliveira, C. 1998, A&AS, 128, 75
Prugniel, P., & Simien, F. 1996, A&A, 309, 749
Puzia, T. H., Kissler-Patig, M., Brodie, J. P., & Huchra, J. P. 1999, AJ, 118, 2734
Reed, L. G., Harris, G. L. H., & Harris, W. E. 1994, AJ, 107, 555
Rhode, K. L., & Zepf, S. E. 2001, AJ, 121, 210
Rieke, G. H., & Lebofsky, M. J. 1985, ApJ, 288, 618
Santiago, B. X., Gilmore, G., & Elson, R. A. W. 1996, MNRAS, 281, 871
Schlegel, D. J., Finkbeiner, D. P., & Davis, M. 1998, ApJ, 500, 525
Silverman, B. W. 1986, Density Estimation for Statistics and Data Analysis (New York: Springer), 18
Thompson, L. A., & Gregory, S. A. 1993, AJ, 106, 2197
Tonry, J. L., Dressler, A., Blakeslee, J. P., Ajhar, E. A., Fletcher, A. B., Luppino, G. A., Metzger, M. R., & Moore, C. B. 2001, ApJ, 546, 681
Woodworth, S. C., & Harris, W. E. 2000, AJ, 119, 2699
Worthey, G. 1994, ApJS, 95, 107
Zepf, S. E., & Ashman, K. M. 1993, MNRAS, 264, 611
Zepf, S. E., Geisler, D., & Ashman, K. M. 1994, ApJ, 435, L117
Zepf, S. E., & Whitmore, B. C. 1993, ApJ, 418, 72